

# Transverse Polarization of $\Lambda$ and $\bar{\Lambda}$ Hyperons in Quasireal Photoproduction

A. Airapetian,<sup>32</sup> N. Akopov,<sup>32</sup> Z. Akopov,<sup>32</sup> M. Amarian,<sup>26,32</sup> V.V. Ammosov,<sup>24</sup> A. Andrus,<sup>15</sup> E.C. Aschenauer,<sup>6</sup> W. Augustyniak,<sup>31</sup> R. Avakian,<sup>32</sup> A. Avetissian,<sup>32</sup> E. Avetissian,<sup>10</sup> P. Bailey,<sup>15</sup> V. Baturin,<sup>23</sup> C. Baumgarten,<sup>21</sup> M. Beckmann,<sup>5</sup> S. Belostotski,<sup>23</sup> S. Bernreuther,<sup>29</sup> N. Bianchi,<sup>10</sup> H.P. Blok,<sup>22,30</sup> H. Böttcher,<sup>6</sup> A. Borissoy,<sup>19</sup> M. Bouwhuis,<sup>15</sup> J. Brack,<sup>4</sup> A. Brüll,<sup>18</sup> I. Brunn,<sup>8</sup> G.P. Capitani,<sup>10</sup> H.C. Chiang,<sup>15</sup> G. Ciullo,<sup>9</sup> M. Contalbrigo,<sup>9</sup> G.R. Court,<sup>16</sup> P.F. Dalpiaz,<sup>9</sup> R. De Leo,<sup>3</sup> L. De Nardo,<sup>1</sup> E. De Sanctis,<sup>10</sup> E. Devitsin,<sup>20</sup> P. Di Nezza,<sup>10</sup> M. Düren,<sup>13</sup> M. Ehrenfried,<sup>6</sup> A. Elalaoui-Moulay,<sup>2</sup> G. Elbakian,<sup>32</sup> F. Ellinghaus,<sup>6</sup> U. Elschenbroich,<sup>11</sup> J. Ely,<sup>4</sup> R. Fabbri,<sup>9</sup> A. Fantoni,<sup>10</sup> A. Fechtchenko,<sup>7</sup> L. Felawka,<sup>28</sup> B. Fox,<sup>4</sup> J. Franz,<sup>11</sup> S. Frullani,<sup>26</sup> Y. Gärber,<sup>8</sup> G. Gapienko,<sup>24</sup> V. Gapienko,<sup>24</sup> F. Garibaldi,<sup>26</sup> E. Garutti,<sup>22</sup> D. Gaskell,<sup>4</sup> G. Gavrillov,<sup>23</sup> V. Gharibyan,<sup>32</sup> G. Graw,<sup>21</sup> O. Grebeniouk,<sup>23</sup> L.G. Greeniaus,<sup>1,28</sup> W. Haeberli,<sup>17</sup> K. Hafidi,<sup>2</sup> M. Hartig,<sup>28</sup> D. Hasch,<sup>10</sup> D. Heesbeen,<sup>22</sup> M. Henoch,<sup>8</sup> R. Hertenberger,<sup>21</sup> W.H.A. Hesselink,<sup>22,30</sup> A. Hillenbrand,<sup>8</sup> Y. Holler,<sup>5</sup> B. Hommez,<sup>12</sup> G. Iarygin,<sup>7</sup> A. Izotov,<sup>23</sup> H.E. Jackson,<sup>2</sup> A. Jgoun,<sup>23</sup> R. Kaiser,<sup>14</sup> E. Kinney,<sup>4</sup> A. Kisselev,<sup>23</sup> K. Königsmann,<sup>11</sup> H. Kolster,<sup>18</sup> M. Kopytin,<sup>23</sup> V. Korotkov,<sup>6</sup> V. Kozlov,<sup>20</sup> B. Krauss,<sup>8</sup> V.G. Krivokhijine,<sup>7</sup> L. Lagamba,<sup>3</sup> L. Lapikás,<sup>22</sup> A. Laziev,<sup>22,30</sup> P. Lenisa,<sup>9</sup> P. Liebing,<sup>6</sup> T. Lindemann,<sup>5</sup> K. Lipka,<sup>6</sup> W. Lorenzon,<sup>19</sup> N.C.R. Makins,<sup>15</sup> H. Marukyan,<sup>32</sup> F. Masoli,<sup>9</sup> F. Menden,<sup>11</sup> V. Mexner,<sup>22</sup> N. Meyners,<sup>5</sup> O. Mikloukho,<sup>23</sup> C.A. Miller,<sup>1,28</sup> Y. Miyachi,<sup>29</sup> V. Muccifora,<sup>10</sup> A. Nagaitsev,<sup>7</sup> E. Nappi,<sup>3</sup> Y. Naryshkin,<sup>23</sup> A. Nass,<sup>8</sup> W.-D. Nowak,<sup>6</sup> K. Oganessyan,<sup>5,10</sup> H. Ohsuga,<sup>29</sup> G. Orlandi,<sup>26</sup> S. Potashov,<sup>20</sup> D.H. Potterveld,<sup>2</sup> M. Raithel,<sup>8</sup> D. Reggiani,<sup>9</sup> P.E. Reimer,<sup>2</sup> A. Reischl,<sup>22</sup> A.R. Reolon,<sup>10</sup> K. Rith,<sup>8</sup> G. Rosner,<sup>14</sup> A. Rostomyan,<sup>32</sup> D. Ryckbosch,<sup>12</sup> I. Sanjiev,<sup>2,23</sup> I. Savin,<sup>7</sup> C. Scarlett,<sup>19</sup> A. Schäfer,<sup>25</sup> C. Schill,<sup>11</sup> G. Schnell,<sup>6</sup> K.P. Schüler,<sup>5</sup> A. Schwind,<sup>6</sup> J. Seibert,<sup>11</sup> B. Seitz,<sup>1</sup> R. Shanidze,<sup>8</sup> T.-A. Shibata,<sup>29</sup> V. Shutov,<sup>7</sup> M.C. Simani,<sup>22,30</sup> K. Sinram,<sup>5</sup> M. Stancari,<sup>9</sup> M. Statera,<sup>9</sup> E. Steffens,<sup>8</sup> J.J.M. Steijger,<sup>22</sup> J. Stewart,<sup>6</sup> U. Stösslein,<sup>4</sup> H. Tanaka,<sup>29</sup> S. Taroian,<sup>32</sup> B. Tchuiko,<sup>24</sup> A. Terkulov,<sup>20</sup> S. Tessarin,<sup>21</sup> E. Thomas,<sup>10</sup> A. Tkabladze,<sup>6</sup> A. Trzcinski,<sup>31</sup> M. Tytgat,<sup>12</sup> G.M. Urciuoli,<sup>26</sup> P.B. van der Nat,<sup>22,30</sup> G. van der Steenhoven,<sup>22</sup> R. van de Vyver,<sup>12</sup> D. Veretennikov,<sup>23</sup> M.C. Vetterli,<sup>27,28</sup> V. Vikhrov,<sup>23</sup> M.G. Vincter,<sup>1</sup> J. Visser,<sup>22</sup> M. Vogt,<sup>8</sup> J. Volmer,<sup>6</sup> C. Weiskopf,<sup>8</sup> J. Wendland,<sup>27,28</sup> J. Wilbert,<sup>8</sup> T. Wise,<sup>17</sup> S. Yen,<sup>28</sup> S. Yoneyama,<sup>29</sup> B. Zihlmann,<sup>22,30</sup> H. Zohrabian,<sup>32</sup> and P. Zupranski<sup>31</sup>

(The HERMES Collaboration)

<sup>1</sup>Department of Physics, University of Alberta, Edmonton, Alberta T6G 2J1, Canada

<sup>2</sup>Physics Division, Argonne National Laboratory, Argonne, Illinois 60439-4843, USA

<sup>3</sup>Istituto Nazionale di Fisica Nucleare, Sezione di Bari, 70124 Bari, Italy

<sup>4</sup>Nuclear Physics Laboratory, University of Colorado, Boulder, Colorado 80309-0390, USA

<sup>5</sup>DESY, 22603 Hamburg, Germany

<sup>6</sup>DESY, 15738 Zeuthen, Germany

<sup>7</sup>Joint Institute for Nuclear Research, 141980 Dubna, Russia

<sup>8</sup>Physikalisches Institut, Universität Erlangen-Nürnberg, 91058 Erlangen, Germany

<sup>9</sup>Istituto Nazionale di Fisica Nucleare, Sezione di Ferrara and

Dipartimento di Fisica, Università di Ferrara, 44100 Ferrara, Italy

<sup>10</sup>Istituto Nazionale di Fisica Nucleare, Laboratori Nazionali di Frascati, 00044 Frascati, Italy

<sup>11</sup>Fakultät für Physik, Universität Freiburg, 79104 Freiburg, Germany

<sup>12</sup>Department of Subatomic and Radiation Physics, University of Gent, 9000 Gent, Belgium

<sup>13</sup>Physikalisches Institut, Universität Gießen, 35392 Gießen, Germany

<sup>14</sup>Department of Physics and Astronomy, University of Glasgow, Glasgow G12 8QQ, United Kingdom

<sup>15</sup>Department of Physics, University of Illinois, Urbana, Illinois 61801-3080, USA

<sup>16</sup>Physics Department, University of Liverpool, Liverpool L69 7ZE, United Kingdom

<sup>17</sup>Department of Physics, University of Wisconsin-Madison, Madison, Wisconsin 53706, USA

<sup>18</sup>Laboratory for Nuclear Science, Massachusetts Institute of Technology, Cambridge, Massachusetts 02139, USA

<sup>19</sup>Randall Laboratory of Physics, University of Michigan, Ann Arbor, Michigan 48109-1040, USA

<sup>20</sup>Lebedev Physical Institute, 117924 Moscow, Russia

<sup>21</sup>Sektion Physik, Universität München, 85748 Garching, Germany

<sup>22</sup>Nationaal Instituut voor Kernfysica en Hoge-Energiefysica (NIKHEF), 1009 DB Amsterdam, The Netherlands

<sup>23</sup>Petersburg Nuclear Physics Institute, St. Petersburg, Gatchina, 188350 Russia

<sup>24</sup>Institute for High Energy Physics, Protvino, Moscow region, 142281 Russia

<sup>25</sup>Institut für Theoretische Physik, Universität Regensburg, 93040 Regensburg, Germany

<sup>26</sup>Istituto Nazionale di Fisica Nucleare, Sezione Roma 1, Gruppo Sanità

and Physics Laboratory, Istituto Superiore di Sanità, 00161 Roma, Italy

<sup>27</sup>Department of Physics, Simon Fraser University, Burnaby, British Columbia V5A 1S6, Canada

<sup>28</sup>TRIUMF, Vancouver, British Columbia V6T 2A3, Canada

<sup>29</sup>*Department of Physics, Tokyo Institute of Technology, Tokyo 152, Japan*

<sup>30</sup>*Department of Physics and Astronomy, Vrije Universiteit, 1081 HV Amsterdam, The Netherlands*

<sup>31</sup>*Andrzej Soltan Institute for Nuclear Studies, 00-689 Warsaw, Poland*

<sup>32</sup>*Yerevan Physics Institute, 375036 Yerevan, Armenia*

The HERMES experiment has measured the transverse polarization of  $\Lambda$  and  $\bar{\Lambda}$  hyperons produced inclusively in quasireal photoproduction at a positron beam energy of 27.6 GeV. The transverse polarization  $P_n^\Lambda$  of the  $\Lambda$  hyperon is found to be positive while the observed  $\bar{\Lambda}$  polarization is compatible with zero. The values averaged over the kinematic acceptance of HERMES are  $P_n^\Lambda = 0.078 \pm 0.006$  (stat)  $\pm 0.012$  (syst) and  $P_n^{\bar{\Lambda}} = -0.025 \pm 0.015$  (stat)  $\pm 0.018$  (syst) for  $\Lambda$  and  $\bar{\Lambda}$ , respectively. The dependences of  $P_n^\Lambda$  and  $P_n^{\bar{\Lambda}}$  on the fraction  $\zeta$  of the beam's light-cone momentum carried by the hyperon and on the hyperon's transverse momentum  $p_T$  were investigated. The measured  $\Lambda$  polarization rises linearly with  $p_T$  and exhibits a different behavior for low and high values of  $\zeta$ , which approximately correspond to the backward and forward regions in the center-of-mass frame of the  $\gamma^*N$  reaction.

PACS numbers: 13.88.+e, 13.60.-r, 13.60.Rj

## INTRODUCTION

In 1976, physicists at Fermilab measured the inclusive production of  $\Lambda$  hyperons from high-energy proton-nucleon scattering, and found a striking result: the  $\Lambda$  particles produced in the forward direction and with transverse momenta greater than about 1 GeV were highly polarized [1]. Both the 300 GeV proton beam and the beryllium target were unpolarized. The  $\Lambda$  polarization was transverse and negative, directed opposite to  $\hat{n}$ , the unit vector along the direction  $\vec{p}_{\text{beam}} \times \vec{p}_\Lambda$ , which is normal to the production plane. This “self-polarization” of final-state hadrons is observed quite commonly in the photoproduction of hyperons at low energies [2, 3], and in exclusive reactions such as elastic  $NN$  or  $\pi N$  scattering [4]. The  $\Lambda$  polarization observable, proportional to  $\vec{S}_\Lambda \cdot \hat{n}$ , where  $\vec{S}_\Lambda$  is the spin vector of the  $\Lambda$ , represents a single-spin asymmetry that is odd under naive time reversal. (Naive time reversal refers to the application of the time reversal operator  $\hat{T}$  to each of the four-momenta in the reaction without exchanging the initial and final states). Given the  $T$ -even nature of the strong and electromagnetic interactions, such a naive  $T$ -odd observable must arise through the interference of two  $T$ -even amplitudes: one that involves a helicity flip and one that does not [5]. The surprise of the Fermilab result was that the polarization also occurred at high energies, in an inclusive measurement with many unobserved particles in the final state. In this regime, perturbative QCD should accurately describe the partonic hard-scattering subprocess  $ab \rightarrow cd$ . However, all helicity-flip amplitudes are greatly suppressed in hard interactions as helicity is conserved in the limit of massless quarks. The mechanism responsible for the polarization must thus arise from the non-perturbative parts of the reaction, such as the fragmentation process  $cd \rightarrow \Lambda X$ . The production of a high-multiplicity final state at high energies must involve a large number of amplitudes. It seems remarkable that the phases of these amplitudes are correlated to such a

degree that a pronounced interference effect is observed.

The polarization of  $\Lambda$  particles and other hyperons has now been observed and investigated in many high-energy scattering experiments, with a wide variety of hadron beams and kinematic settings [6, 7, 8, 9]. The polarization of  $\Lambda$  particles in particular is almost always found to be negative, as in the original  $pN$  experiment. A notable exception to this rule is the positive polarization measured in  $K^-p$  [10] and  $\Sigma^-N$  [8] interactions, where the beam particles contain valence  $s$  quarks. A rather consistent kinematic behavior of the polarization has been observed: its magnitude increases almost linearly with the transverse momentum  $p_T$  of the  $\Lambda$  hyperon up to a value of about 1 GeV, where a plateau is reached. The absolute polarization also rises with the Feynman variable  $x_F$  with values around 0.3 at  $x_F \approx 0.7$ .

Possible mechanisms for the origin of this polarization were reviewed in Refs. [11] and [12] for example. None of these models was able to account for the complete set of available measurements. In particular, no model could explain the baffling pattern of anti-hyperon polarization. Anti-hyperons produced in  $pN$  scattering contain no valence quarks in common with the beam and are expected to have no polarization. Zero polarization has indeed been consistently measured in the reaction  $pN \rightarrow \bar{\Lambda}X$ . However, studies of the reactions  $pN \rightarrow \bar{\Xi}^- X$  and  $pp \rightarrow \bar{\Sigma}^+ X$  revealed anti-hyperon polarizations of the same sign and magnitude as those of the corresponding hyperons [13]. These observations have presented a decade-long puzzle in non-perturbative QCD. To our knowledge only one possible solution has been suggested [14] so far.

Given the large hyperon polarization observed in hadron-scattering experiments, it is natural to wonder whether a non-vanishing polarization also occurs in  $\Lambda$  production by real and virtual photons at high energies. Very little experimental information exists about this effect in photo- and electroproduction. Transverse polarization in the inclusive photoproduction of neutral

strange particles was investigated about 20 years ago at CERN [15] and SLAC [16]. However, the statistical accuracy of these data is limited. The CERN measurements, for incident tagged photons with energies between 25 and 70 GeV, resulted in an average polarization of  $0.06 \pm 0.04$ . At SLAC, the overall polarization was observed to be  $0.09 \pm 0.07$  for  $\Lambda$  hyperons produced using a 20 GeV photon beam. The SLAC experiment also investigated the dependence of the polarization on  $x_F$  and observed a decrease, with the polarization tending towards negative values for positive  $x_F$ .

## EXPERIMENT

The HERMES experiment offers an excellent opportunity to measure transverse  $\Lambda$  and  $\bar{\Lambda}$  polarization in the reaction  $\gamma^* N \rightarrow \bar{\Lambda} X$ , using the 27.6 GeV positron beam of the HERA collider and an internal gas target. For simplicity the symbol  $\Lambda$  will henceforward be used to refer to both the  $\Lambda$  and  $\bar{\Lambda}$  cases unless explicitly stated otherwise. The HERMES detector [17] is a magnetic spectrometer whose geometric acceptance is confined to two regions in scattering angle, arranged symmetrically above and below the beam pipe. These regions are defined by the rectangular pole gaps in the spectrometer magnet, and cover the ranges  $\pm(40\text{--}140)$  mrad in the vertical component of the scattering angle and  $\pm 170$  mrad in the horizontal component. Between these regions is the horizontal septum plate of the magnet, which shields the HERA beams from the spectrometer's dipole field. Thus, only particles produced with a polar angle greater than 40 mrad with respect to the beam axis are visible. Since the standard HERMES trigger for deep-inelastic reactions requires an energy of more than 1.4 GeV or often even 3.5 GeV deposited in a lead-glass electromagnetic calorimeter, scattered positrons may be detected only for events with  $Q^2$  above about 0.1 GeV<sup>2</sup> (where  $-Q^2$  represents the four-momentum squared of the virtual photon). In the study described in this paper, the detection of the scattered positron was not required and the final data sample is therefore dominated by the kinematic regime  $Q^2 \approx 0$  GeV<sup>2</sup> of quasireal photoproduction where the cross section is largest. The scattered beam positron was detected in coincidence with a  $\Lambda$  in only 6% of the events.

A Monte Carlo simulation of the process using the PYTHIA event generator [18] and a GEANT [19] model of the detector was used to estimate the average kinematics of the  $\Lambda$  sample. An average virtual photon energy of  $\langle \nu \rangle \approx 16$  GeV was obtained. A total of about 70% of the detected  $\Lambda$  events lie below  $Q^2$  of 0.01 GeV<sup>2</sup>, and about 90% lie below 0.5 GeV<sup>2</sup>. Due to the long tail at higher values in the  $Q^2$  distribution, the average  $Q^2$  value is not representative of the typical event kinematics. The measurement is thus kinematically comparable to those at

CERN and SLAC, while offering a much higher statistical precision. However, unlike in these two experiments, the kinematics of the quasireal photons are not known on an event-by-event basis.

This analysis combines the data collected at HERMES in the years 1996 – 2000. The sample includes data taken with both longitudinally polarized and unpolarized targets, while the positron beam was always longitudinally polarized. As the target spin direction was reversed every 90 seconds, the average target polarization was negligibly small. The target species included hydrogen, deuterium, and a variety of unpolarized heavier gases.

## EXTRACTION OF THE TRANSVERSE POLARIZATION

Because of the parity-conserving nature of the strong interaction, any final-state hadron polarization in a reaction with unpolarized beam and target must point along a pseudo-vector direction. In the case of inclusive hyperon production, the only available direction of this type is the normal  $\hat{n}$  to the production plane formed by the cross-product of the vectors along the laboratory-frame momenta of the positron beam ( $\vec{p}_e$ ) and the  $\Lambda$  ( $\vec{p}_\Lambda$ ):

$$\hat{n} = \frac{\vec{p}_e \times \vec{p}_\Lambda}{|\vec{p}_e \times \vec{p}_\Lambda|}. \quad (1)$$

By the same parity conservation argument, the polarization in this transverse (i.e., normal) direction cannot depend linearly on the longitudinal polarization of the target ( $P_T$ ) or the beam ( $P_B$ ). A dependence on their product  $P_T P_B$ , however, is not forbidden. In this analysis most of the  $\Lambda$  data were collected using unpolarized targets, and the luminosity weighted value of  $P_B P_T$  was  $0.0000 \pm 0.0005$  for the entire data sample.

A kinematic diagram of inclusive  $\Lambda$  production and the decay  $\Lambda \rightarrow p\pi^-$  is given in Fig. 1. The  $\Lambda$  decay is shown in the  $\Lambda$  rest frame, where  $\theta_p$  (see Eq. 3) is the angle of proton emission relative to the axis given by the normal  $\hat{n}$  to the scattering plane. Although  $\hat{n}$  is defined in Eq. 1 using vectors in the laboratory frame, it is important to note that the direction is unaffected by the boost into the  $\Lambda$  rest frame.

The  $\Lambda$  hyperon is a uniquely useful particle in spin physics: the parity-violating nature of its weak decay  $\Lambda \rightarrow p\pi^-$  results in an angular distribution where the protons are preferentially emitted along the spin direction of their parent  $\Lambda$ . The angular distribution of the decay products of the  $\Lambda$  may thus be used to measure its polarization, providing a rare opportunity to explore spin degrees of freedom in the fragmentation process. In the rest frame of the  $\Lambda$  it has the form

$$\frac{dN}{d\Omega_p} = \frac{dN_0}{d\Omega_p} (1 + \alpha \vec{P}^\Lambda \cdot \hat{k}_p). \quad (2)$$

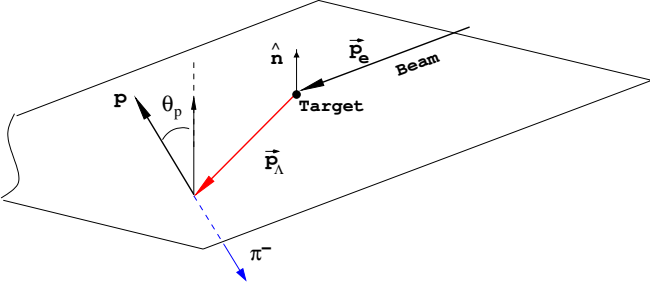


FIG. 1: Schematic diagram of inclusive  $\Lambda$  production and decay. The angle  $\theta_p$  of the decay proton with respect to the normal  $\hat{n}$  to the production plane is defined in the  $\Lambda$  rest frame.

Here,  $\hat{k}_p$  is the proton momentum unit vector in the  $\Lambda$  rest frame,  $\vec{P}^\Lambda$  is the polarization of the  $\Lambda$ , and  $\alpha = 0.642 \pm 0.013$  is the analyzing power of the parity-violating weak decay [20]. Assuming  $CP$ -invariance of the decay, the analyzing power for the  $\bar{\Lambda}$  is of opposite sign ( $\alpha^{\bar{\Lambda}} = -0.642$ ) [20]. The quantity  $dN_0/d\Omega_p$  denotes the decay distribution of *unpolarized*  $\Lambda$  particles. As described above, only the normal component  $P_n^\Lambda$  of the  $\Lambda$  polarization may be non-zero in the present analysis, and so Eq. 2 may be rewritten as

$$\frac{dN}{d\Omega_p} = \frac{dN_0}{d\Omega_p} (1 + \alpha P_n^\Lambda \cos \theta_p). \quad (3)$$

For unpolarized  $\Lambda$  particles the distribution of the decay particles is isotropic and  $dN_0/d\Omega_p$  is simply a normalization factor, independent of angle. In the case of limited spectrometer acceptance, however, it acquires a dependence on  $\cos \theta_p$ .

To extract the polarization of a sample of  $\Lambda$  hyperons from the angular distribution of their decay products in the acceptance, one may determine the following moments:

$$\langle \cos^m \theta_p \rangle \equiv \frac{\int \cos^m \theta_p \frac{dN}{d\Omega_p} d\Omega_p}{\int \frac{dN}{d\Omega_p} d\Omega_p} \equiv \frac{\int \cos^m \theta_p \frac{dN_0}{d\Omega_p} d\Omega_p}{N_{\text{acc}}^\Lambda}, \quad (4)$$

and

$$\langle \cos^m \theta_p \rangle_0 \equiv \frac{\int \cos^m \theta_p \frac{dN_0}{d\Omega_p} d\Omega_p}{\int \frac{dN_0}{d\Omega_p} d\Omega_p} \equiv \frac{\int \cos^m \theta_p \frac{dN_0}{d\Omega_p} d\Omega_p}{N_{0,\text{acc}}^\Lambda}, \quad (5)$$

where  $m = 1, 2, \dots$ . The symbol  $\langle \dots \rangle$  represents an average over an actual data sample, while  $\langle \dots \rangle_0$  denotes an average over a hypothetical purely-unpolarized sample of  $\Lambda$  particles with an isotropic decay distribution.  $N_{\text{acc}}^\Lambda$  and  $N_{0,\text{acc}}^\Lambda$  are equal to the total number of  $\Lambda$  events for the same luminosity accepted by the spectrometer. They are related by

$$N_{\text{acc}}^\Lambda = N_{0,\text{acc}}^\Lambda (1 + \alpha P_n^\Lambda \langle \cos \theta_p \rangle_0). \quad (6)$$

Combining Eqs. 3 - 6 one obtains

$$\langle \cos^m \theta_p \rangle = \frac{\langle \cos^m \theta_p \rangle_0 + \alpha P_n^\Lambda \langle \cos^{m+1} \theta_p \rangle_0}{1 + \alpha P_n^\Lambda \langle \cos \theta_p \rangle_0}. \quad (7)$$

The extraction of the  $\Lambda$  polarization  $P_n^\Lambda$  from the experimental data is based on Eq. 7. The ‘polarized’ moments  $\langle \cos^m \theta_p \rangle$  can be determined by taking an average over the experimental data set:

$$\langle \cos^m \theta_p \rangle = \frac{1}{N_{\text{acc}}^\Lambda} \sum_{i=1}^{N_{\text{acc}}^\Lambda} \cos^m \theta_{p,i}. \quad (8)$$

The ‘unpolarized’ moments  $\langle \cos^m \theta_p \rangle_0$  cannot be extracted directly from the data as no sample of unpolarized  $\Lambda$  hyperons is available. Fortunately, however, the extraction of the transverse  $\Lambda$  polarization from the HERMES data is greatly simplified by the up/down mirror symmetry of the HERMES spectrometer, even in the case of limited acceptance. It can be readily shown that this geometric symmetry leads to the relation

$$\langle \cos^m \theta_p \rangle_0^{\text{top}} = (-1)^m \langle \cos^m \theta_p \rangle_0^{\text{bot}}, \quad (9)$$

where *top* and *bot* specify events in which the hyperon’s momentum was directed above or below the midplane of the spectrometer. Consequently all ‘unpolarized’ uneven moments of the full acceptance function (*top* plus *bot*) are zero, and all even ‘polarized’ moments are equal to the ‘unpolarized’ ones:

$$\langle \cos^m \theta_p \rangle = \langle \cos^m \theta_p \rangle_0 \quad m = 2, 4, \dots \quad (10)$$

The first moment of  $\cos \theta_p$  may be calculated separately for the *top* and *bot* data samples to account for a possible difference in the overall efficiency of each detector half. Using the symmetry relations (Eqs. 9 and 10), one obtains from Eq. 7 a system of two coupled equations for  $\alpha P_n^\Lambda$  and  $\langle \cos \theta_p \rangle_0^{\text{top}}$ :

$$\alpha P_n^\Lambda = \frac{c_+ / \langle \cos^2 \theta_p \rangle}{1 - \langle \cos \theta_p \rangle_0^{\text{top}} c_- / \langle \cos^2 \theta_p \rangle}, \quad (11)$$

$$\langle \cos \theta_p \rangle_0^{\text{top}} = \frac{c_-}{1 - c_+ \alpha P_n^\Lambda}, \quad (12)$$

where  $2c_+$  ( $2c_-$ ) is the sum (difference) of  $\langle \cos \theta_p \rangle_0^{\text{top}}$  and  $\langle \cos \theta_p \rangle_0^{\text{bot}}$ . This system of coupled equations can be solved iteratively. The iteration converges quickly. If one takes  $\alpha P_n^\Lambda = c_+ / \langle \cos^2 \theta_p \rangle$  and  $\langle \cos \theta_p \rangle_0^{\text{top}} = c_-$  for the first iteration, then the solution of the second iteration for  $P_n^\Lambda$  and  $\langle \cos \theta_p \rangle_0^{\text{top}}$  reads:

$$\alpha P_n^\Lambda = \frac{c_+ / \langle \cos^2 \theta_p \rangle}{1 - c_-^2 / \langle \cos^2 \theta_p \rangle}, \quad (13)$$

$$\langle \cos \theta_p \rangle_0^{\text{top}} = \frac{c_-}{1 - c_+^2 / \langle \cos^2 \theta_p \rangle}. \quad (14)$$

Eq. 13 was used to determine the results presented in this paper.

The results for the ‘unpolarized’ first moment of  $\cos\theta_p$  determined in various kinematic bins from data were found to be in very good agreement with those obtained from a Monte Carlo simulation of the detector.

## EVENT SELECTION

The kinematics of the  $\Lambda$  hyperons whose decay products are both within the angular acceptance of the HERMES spectrometer are such that the proton momentum is always much higher than that of the pion. These low-momentum pions are often bent so severely in the spectrometer magnet that they fail to reach the tracking chambers and particle identification detectors in the backward half of the spectrometer. However, it is possible to evaluate the momentum of such ‘short tracks’ using the hits recorded by the HERMES Magnet Chambers, a series of proportional chambers located between the poles of the spectrometer magnet [21]. The acceptance for  $\Lambda$  hyperons can be increased by almost a factor of two when these pion ‘short tracks’ are included in the analysis. As non-pions in coincidence with protons are rare, particle identification (PID) is not essential for these tracks. In contrast, PID of the decay proton is important for background reduction. For the data recorded prior to 1998, this was provided by a threshold Čerenkov counter [17], which was then replaced by a dual-radiator Ring-Imaging Čerenkov detector (RICH) [22]. Proton candidates were therefore required to be a positive hadron with the highest-momentum (leading hadron) having a ‘long track’, i.e., a track that passed through all detectors of the spectrometer, and to be not identified as a pion.

$\Lambda$  events were identified through the reconstruction of secondary vertices in events containing oppositely charged hadron pairs. Two spatial vertices were reconstructed for each event. First the secondary (decay) vertex was determined from the intersection (i.e., point of closest approach) of the proton and pion tracks. The hyperon track was then reconstructed using this decay vertex and the sum of the proton and pion 3-momenta. The intersection of this track with the beam axis determined the primary (production) vertex. For both vertices the distance of closest approach was required to be less than 1.5 cm. Only those events with the primary vertex inside the 40 cm long target cell were selected. All tracks were also required to satisfy a series of fiducial-volume cuts designed to avoid the edges of the detector. Furthermore the two hadron tracks were required to be reconstructed in the same spectrometer half to avoid effects caused by a possible misalignment of the two spectrometer halves relative to each other.

Hadrons emitted from the primary vertex were sup-

pressed by two vertex separation requirements. The transverse distance between the decay vertex and the beam axis was required to be larger than 1 cm. In the longitudinal direction the requirement  $z_2 - z_1 > 15(20)$  cm was imposed for  $\Lambda$  candidates, with  $z_1$  and  $z_2$  representing the coordinates of the primary and secondary vertex positions along the beam direction. The chosen values of this vertex separation requirement were a compromise between statistical precision and low background of the data sample.

The resulting  $p\pi^-$  and  $\bar{p}\pi^+$  invariant mass distributions are shown in Fig. 2. The fitted mean value for the  $\Lambda$  ( $\bar{\Lambda}$ ) mass is 1.1157 GeV (1.1156 GeV) with a width of  $\sigma = 2.23$  MeV (2.20 MeV). For the polarization analysis,  $\Lambda$  and  $\bar{\Lambda}$  events within a  $\pm 3.3\sigma$  invariant mass window around the mean value of the fitted peak were chosen, and a background-subtraction procedure was applied as described below. The final data sample contained around  $259 \times 10^3$   $\Lambda$  and  $51 \times 10^3$   $\bar{\Lambda}$  events.

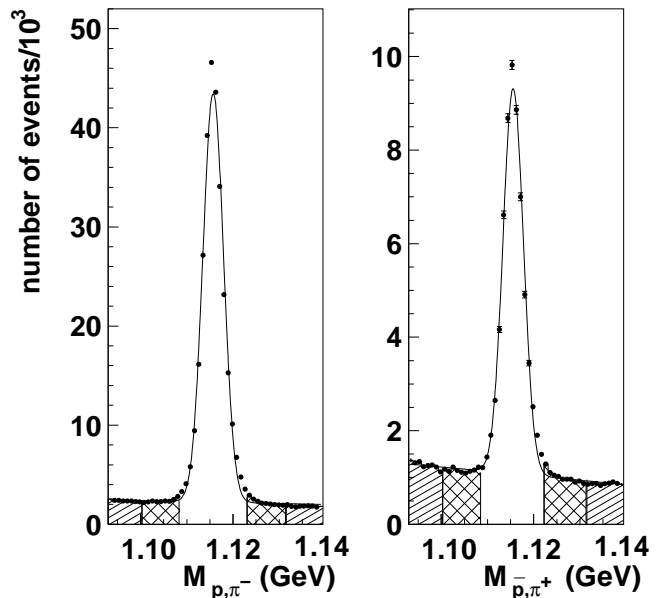


FIG. 2: Invariant mass distributions for  $\Lambda$  and  $\bar{\Lambda}$  events. The central region was used for the determination of the  $\Lambda$  ( $\bar{\Lambda}$ ) polarization. The shaded areas indicate the invariant-mass intervals used for the determination of the background polarization.

## RESULTS

The transverse polarization for the  $\Lambda$  and  $\bar{\Lambda}$  data samples was extracted using Eq. 13. The contribution of the background under the  $\Lambda$  invariant mass peak to the polarization was estimated using a side-band subtraction method. An independent polarization analysis was performed in each kinematic bin of interest. For each bin

in  $\zeta$  or  $p_T$  (described below), the invariant mass spectrum was fit with a Gaussian plus a third-order polynomial. The fit was used to determine the number of signal and background events within a  $\pm 3.3\sigma$  window around the peak. The polarization was calculated for the events within this central window, as well as within four “side-band” windows with widths of around 8 MeV, two in the low- and two in the high-mass background regions, as indicated by the shaded areas in Fig. 2. The polarizations extracted from the sidebands were interpolated to obtain the background polarization at the peak mass. The fraction of background events  $\epsilon = \frac{N_{bgr}}{N_\Lambda + N_{bgr}}$  within the peak was typically of order 15 %. The transverse polarization within the  $\Lambda$  peak was corrected for this background contribution in each kinematic bin as follows

$$P_n^\Lambda = \frac{P_n^{\Lambda+bgr} - \epsilon P_n^{bgr}}{1 - \epsilon}. \quad (15)$$

The interpolated background polarization  $P_n^{bgr}$  was around  $0.12 \pm 0.01$  ( $0.13 \pm 0.02$ ) for the  $\Lambda$  ( $\bar{\Lambda}$ ) sample. Because of the small background contamination, the net correction to the  $\Lambda$  and  $\bar{\Lambda}$  polarization was on average below 0.01. The results for the extracted value of the transverse  $\Lambda$  polarization were stable within the statistical uncertainty when the longitudinal vertex separation requirement was varied between 10 and 25 cm.

In order to estimate the systematic uncertainty of the measurement, similar analyses were carried out for reconstructed  $h^+h^-$  hadron pairs, with leading positive hadrons ( $\Lambda$ -like case) and with leading negative hadrons ( $\bar{\Lambda}$ -like case). No PID (apart from lepton rejection) was applied to these hadrons, and so the sample was likely dominated by  $\pi^+\pi^-$  pairs. Events within two mass windows above and below the  $\Lambda$  mass window ( $1.093 \text{ GeV} < M_{h^+h^-} < 1.108 \text{ GeV}$ , and  $1.124 \text{ GeV} < M_{h^+h^-} < 1.139 \text{ GeV}$ ) were selected, where  $M_{h^+h^-}$  was determined by assuming for the leading/non-leading particles the proton/pion masses respectively. Instead of requiring a displaced decay vertex, their point of closest approach was required to be inside the target cell. False polarization values of  $0.012 \pm 0.002$  and  $0.018 \pm 0.002$  were found in the  $\Lambda$ -like and  $\bar{\Lambda}$ -like cases, respectively.

As a second measure of the systematic uncertainty a sample of  $K_s^0 \rightarrow \pi^+ \pi^-$  events was used. The long-lived  $K_s^0$  provides a similar event topology to the  $\Lambda$  with two separated vertices. The false polarization of  $K_s^0$  was found to be  $0.012 \pm 0.004$  in the  $\Lambda$ -like case (with a leading  $\pi^+$ ) and  $0.002 \pm 0.004$  in the  $\bar{\Lambda}$ -like case.

Possible detector misalignments could lead to imperfections in the up/down symmetry of the spectrometer. In order to estimate the effect of such misalignments on the measured polarizations, Monte Carlo simulations were performed using a spectrometer description with the top and bottom halves misaligned by  $\pm 0.5$  mrad. Four samples were generated, with input polarizations of 0,

0.05, 0.1 and 0.2, respectively. In addition a background polarization of 0.15 was included to better simulate the experimental situation. The polarizations extracted from these Monte Carlo data samples were in agreement with the input values within the statistical uncertainty of 0.005. A second potential source of a top/bottom spectrometer asymmetry is trigger inefficiency. This was also investigated using Monte Carlo simulations. It was found that even an unrealistically large difference of 30% in the top/bottom efficiency resulted in the reconstructed polarization being consistent with the generated one.

From the results of these studies the systematic uncertainties on the  $\Lambda$  and  $\bar{\Lambda}$  transverse polarizations were taken to be 0.012 and 0.018, respectively.

The good statistical accuracy of the full inclusive data set allows the dependence of the  $\Lambda$  and  $\bar{\Lambda}$  polarization on certain kinematic variables to be studied. As mentioned earlier, information on the virtual-photon kinematics is not known on an event-by-event basis; consequently, only kinematic variables related to the  $eN$  system are available. However, one may analyze the data using the kinematic variable  $\zeta \equiv (E_\Lambda + p_{z\Lambda})/(E_e + p_e)$ , where  $E_\Lambda$ ,  $p_{z\Lambda}$  are the energy and  $z$ -component of the  $\Lambda$  momentum (where the  $z$ -axis is defined as the lepton beam direction), and  $E_e$ ,  $p_e$  are the energy and momentum of the positron beam. This variable is the fraction of the beam positron’s light-cone momentum carried by the outgoing  $\Lambda$ . It is an approximate measure of whether the hyperons were produced in the forward or backward region in the  $\gamma^*N$  center-of-mass system. The natural variable to use to separate these kinematic regimes would be the Feynman variable  $x_F = p_{\parallel}^\Lambda/p_{\parallel\text{max}}^\Lambda$  evaluated in the  $\gamma^*N$  system, where  $p_{\parallel}^\Lambda$  is the  $\Lambda$ ’s momentum along the virtual-photon direction, and  $p_{\parallel\text{max}}^\Lambda$  is its maximum possible value, but this variable is not available in an inclusive measurement. Nevertheless, as shown in Fig. 3, a simulation of the reaction using the PYTHIA Monte Carlo reveals a useful correlation between  $\zeta$  and  $x_F$ . In particular, all events at  $\zeta \geq 0.25$  are produced in the kinematic region  $x_F > 0$ , and for  $\zeta < 0.25$  there is a mixture of events originating from the kinematic regions with  $x_F > 0$  and  $x_F < 0$ . An indication that the dominant production mechanism changes at  $\zeta$  values around 0.25 can be observed in the ratio of  $\Lambda$  to  $\bar{\Lambda}$  yields displayed in Fig. 4. The yields are not corrected for acceptance as PYTHIA Monte Carlo studies indicate that the detection efficiencies for  $\Lambda$  and  $\bar{\Lambda}$  are the same. Above  $\zeta \approx 0.25$ , an approximately constant ratio of about 4 is seen. At lower values the ratio increases significantly, likely indicating the influence of the nucleon target remnant in  $\Lambda$  formation.

The  $\Lambda$  and  $\bar{\Lambda}$  polarizations are shown as functions of  $\zeta$  in Fig. 5. The  $\Lambda$  polarization is about 0.10 in the region  $\zeta < 0.25$ , and about 0.05 at higher  $\zeta$ . Combining all kinematic points together, the average  $\Lambda$  transverse

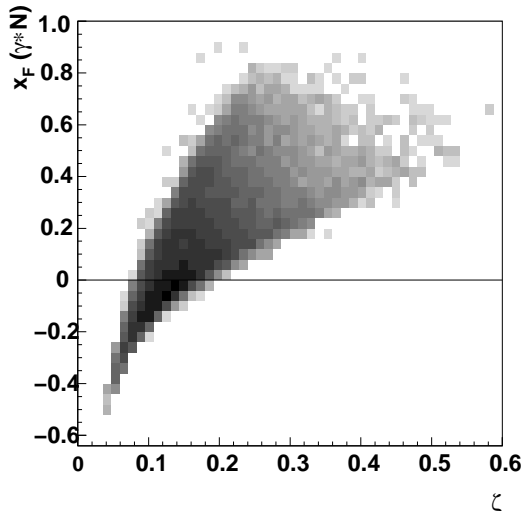


FIG. 3: Correlation between  $x_F$ , evaluated in the  $\gamma^*N$  system, and the light-cone fraction  $\zeta$  determined in the  $eN$  system, as determined from a PYTHIA Monte Carlo simulation.

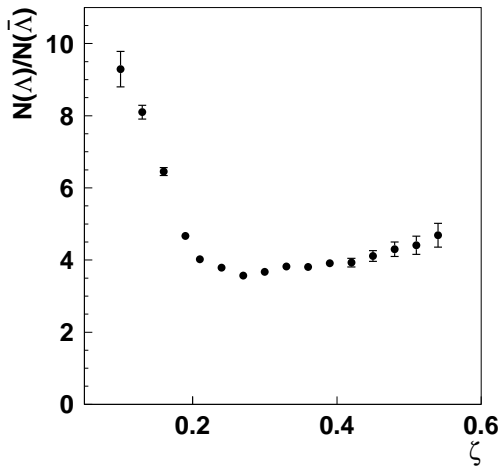


FIG. 4: Ratio of  $\Lambda$  to  $\bar{\Lambda}$  yields versus light-cone fraction  $\zeta$  observed in the data, after background subtraction.

polarization is

$$P_n^\Lambda = 0.078 \pm 0.006(\text{stat}) \pm 0.012(\text{syst}). \quad (16)$$

For the  $\bar{\Lambda}$  measurement, no kinematic dependence is observed within the statistical uncertainties. The net  $\bar{\Lambda}$  transverse polarization is

$$P_n^{\bar{\Lambda}} = -0.025 \pm 0.015(\text{stat}) \pm 0.018(\text{syst}). \quad (17)$$

It should be noted that for each point in  $\zeta$  the value of the hyperon's mean transverse momentum  $\langle p_T \rangle$  is different as is shown in the lower panel of Fig. 5. Here  $p_T$  is defined with respect to the  $eN$  system rather than to the  $\gamma^*N$  system as, again, the virtual-photon direction

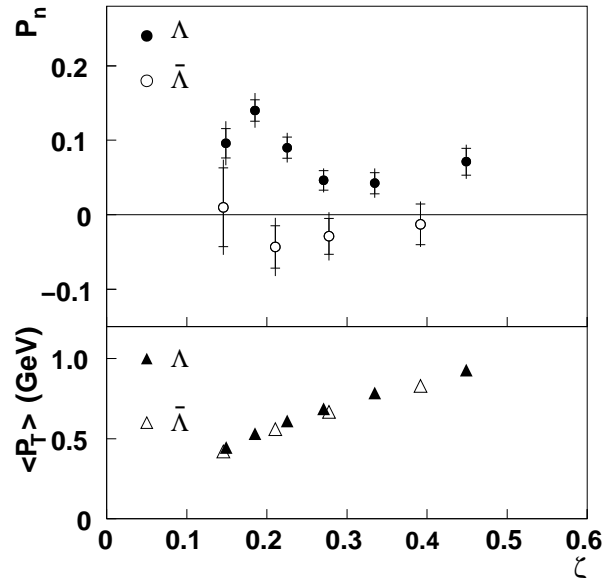


FIG. 5: Transverse polarizations  $P_n^\Lambda$  and  $P_n^{\bar{\Lambda}}$  (upper panel) and mean  $\langle p_T \rangle$  (lower panel) as functions of  $\zeta = (E_\Lambda + p_{z\Lambda})/(E_e + p_e)$ . The inner error bars represent the statistical uncertainties, and the outer error bars represent the statistical and systematic uncertainties added in quadrature.

was not determined in this inclusive analysis. In Fig. 6, the transverse  $\Lambda$  and  $\bar{\Lambda}$  polarizations are shown versus  $p_T$  for the two intervals  $\zeta < 0.25$  and  $\zeta > 0.25$ . In both regimes the  $\Lambda$  polarization rises linearly with  $p_T$ , resembling the linear rise of hyperon polarization magnitude with  $p_T$  that was consistently observed in the forward production of hyperons in hadronic reactions. For the  $\bar{\Lambda}$ , again no kinematic dependence of the polarization is observed within statistics.

## DISCUSSION

The transverse  $\Lambda$  polarization measured by HERMES in the  $\gamma^*N \rightarrow \Lambda X$  reaction is positive, in contrast to the negative values observed in almost all other reactions. Very few theoretical models of the kinematic dependence of  $\Lambda$  polarization in photo- or electroproduction are available for comparison with the data. Negative transverse  $\Lambda$  and  $\bar{\Lambda}$  polarizations were predicted for the electroproduction case in Ref. [23], where transverse  $\Lambda$  polarization is associated with the  $T$ -odd fragmentation function  $D_{1T}^\perp(z, Q^2)$ , one of eight fragmentation functions identified in a complete tree-level analysis of semi-inclusive deep-inelastic scattering [24]. However, these calculations are confined to the high- $Q^2$  regime of deep-inelastic scattering.

One may speculate on the reason for the positive  $\Lambda$  polarization in  $\gamma^*N \rightarrow \Lambda X$ . In the model given in Ref. [25], for example, forward-going  $\Lambda$  particles pro-

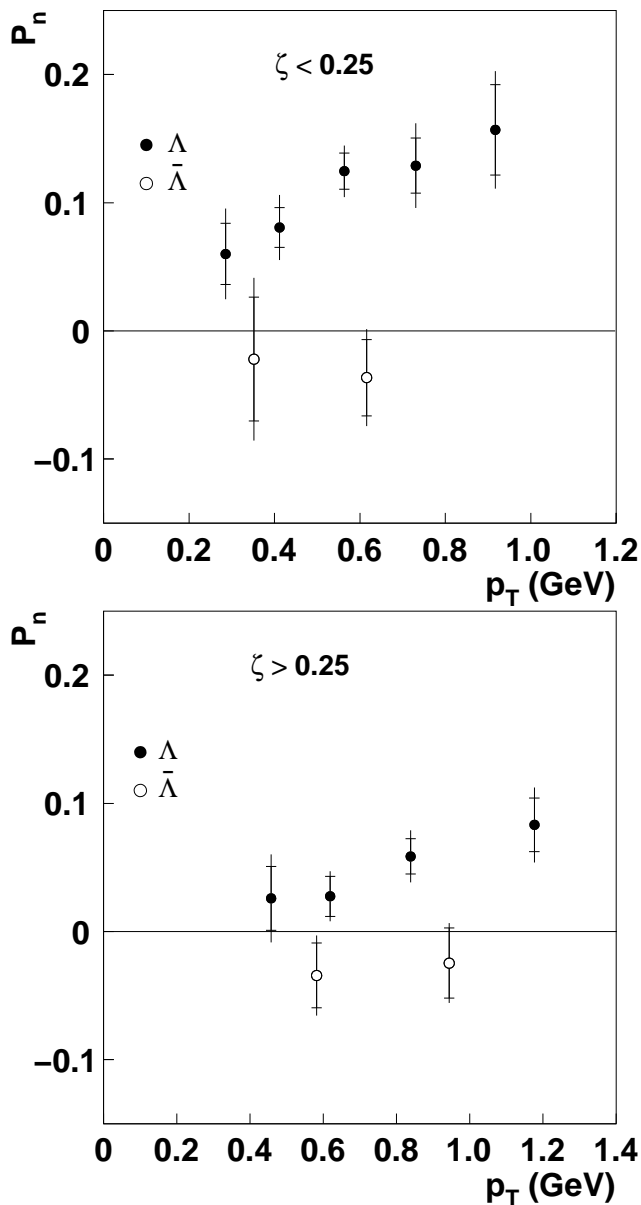


FIG. 6: Transverse polarizations  $P_n^\Lambda$  and  $P_n^{\bar{\Lambda}}$  as a function of  $p_T$  for hyperons from the region  $\zeta < 0.25$  (upper panel) and the region  $\zeta > 0.25$  (lower panel). The inner error bars represent the statistical uncertainties, and the outer error bars represent the statistical and systematic uncertainties added in quadrature.

duced in proton-proton scattering are formed from the recombination of a high-momentum spin- and isospin-singlet  $ud$  diquark from the beam with a strange sea quark from the target or the fragmentation process. The negative  $\Lambda$  polarization then arises from the acceleration of the strange quark, via the Thomas precession effect. Conversely, the positive  $\Lambda$  polarization observed with  $K^-$  and  $\Sigma^-$  beams is indicative of the deceleration of strange quarks from the beam. The positive polarization observed in the HERMES quasireal photoproduction data

might therefore indicate that the  $\gamma \rightarrow s\bar{s}$  hadronic component of the photon plays a significant role in inclusive  $\Lambda$  production.

The different average magnitude of  $P_n^\Lambda$  for  $\zeta$  below and above 0.25 and the increase of the ratio of  $\Lambda$  to  $\bar{\Lambda}$  yields at low values of  $\zeta$  might be an indication of different hyperon formation mechanisms in the “backward” and “forward” kinematic regions, i.e., recombination of a quark from the beam with a diquark from the target in the “backward” region, and with a diquark from a string-break in the “forward” region.

The positive transverse polarization of  $\Lambda$  hyperons has indeed been explained in a quark-recombination model [26], in which  $u$ ,  $d$  and  $s$  quarks from the  $\gamma$  beam contribute to the  $\Lambda$  production and polarization through the recombinations  $s + (ud)^0$ ,  $u + (ds)^{0,1}$  and  $d + (us)^{0,1}$ , where the upper indices 0 (1) correspond to singlet (triplet) diquark configurations. The contributions of the latter two recombinations are suppressed due to the higher mass of the diquarks containing an  $s$  quark.

In the framework of impact-parameter-dependent generalized parton distribution functions, it was argued in Ref. [27] that  $\Lambda$  hyperons produced in the collision of a beam containing  $s$  quarks with a nucleon target have a positive transverse polarization. In this work, a similar mechanism was also used to explain another  $T$ -odd observable, the so-called Sivers asymmetry in electroproduction of pions as observed at HERMES [28].

As no theory is currently able to explain the existing body of  $\Lambda$  polarization data, all such model-dependent speculations must be viewed only as exploratory considerations. The result presented here, a first measurement of non-zero transverse polarization in the  $\gamma^*N \rightarrow \Lambda X$  reactions at  $Q^2 \approx 0$ , adds an interesting new piece to the long-standing mystery of hyperon polarization at high energies.

We gratefully acknowledge the DESY management for its support and the DESY staff and the staffs of the collaborating institutions. This work was supported by the Ministry of Education and Science of Armenia; the FWO-Flanders, Belgium; the Natural Sciences and Engineering Research Council of Canada; the INTAS and RTN network ESOP contributions from the European Union; the European Commission IHP program; the German Bundesministerium für Bildung und Forschung (BMBF); the Deutsche Forschungsgemeinschaft (DFG); the Italian Istituto Nazionale di Fisica Nucleare (INFN); Monbusho International Scientific Research Program, JSPS, and Toray Science Foundation of Japan; the Dutch Foundation for Fundamenteel Onderzoek der Materie (FOM); the Russian Academy of Science and the Russian Federal Agency for Science and Innovations; the U.K. Particle Physics and Astronomy Research Council; and the U.S. Department of Energy (DOE) and the National Science Foundation (NSF).



- 
- [1] G. Bunce *et al.*, Phys. Rev. Lett **36**, 1113 (1976).
- [2] M. Bockhorst *et al.*, Zeit. Phys. C **63**, 37 (1994); SAPHIR Collaboration, M.Q. Tran *et al.*, Phys. Lett. B **445**, 20 (1998).
- [3] CLAS Collaboration, J.W.C. McNabb *et al.*, Phys. Rev. C **69**, 042201 (2004).
- [4] C. Bourrely, E. Leader, and J. Soffer, Phys. Rep. **59**, 95 (1980).
- [5] S. Gasiorowicz, “Elementary Particle Physics” (John Wiley & Sons, 1966), p. 515; N.H. Buttimore, E. Gotsman, and E. Leader, Phys. Rev. D **18**, 694 (1978); M.L. Goldberger, M.T. Grisaru, S.W. MacDowell, and D.Y. Wong, Phys. Rev. **120**, 2250 (1960).
- [6] K. Heller, in “Proceedings of the 12<sup>th</sup> International Symposium on High-Energy Spin Physics (SPIN 96)”, edited by C.W. de Jager, T.J. Ketel, P.J. Mulders, J.E.J. Ober-ski, M. Oskam-Tamboezer (World Scientific, Singapore, 1997), p.23.
- [7] J. Lach, Nucl. Phys. (Proc. Suppl.) **50**, 216 (1996).
- [8] WA89 Collaboration, M.I. Adamovich *et al.*, Eur. Phys. J. C **32**, 221 (2004).
- [9] HERA-B Collaboration, I. Abt *et al.*, Phys. Lett. B **638**, 415 (2006).
- [10] S. Gourlay *et al.*, Phys. Rev. Lett **56**, 2214 (1986).
- [11] A.D. Panagiotou, Int. J. Mod. Phys. **A5**, 1197 (1990).
- [12] J. Soffer, in “Proceedings of the Hyperon Physics Symposium on High-Energy (Hyperon 99)”, edited by D.A. Jensen and E. Monnier (Fermi National Accelerator Laboratory, Batavia, Ill, 1999), p.121.
- [13] FNAL-E756 Collaboration, P. Ho *et al.*, Phys. Rev. Lett **65**, 1713 (1990); FNAL-E761 Collaboration, A. Morelos *et al.*, Phys. Rev. Lett **71**, 2172 (1993).
- [14] K. Kubo, Y. Yamamoto, and H. Toki, Prog. Theor. Phys. **101**, 615 (1999).
- [15] CERN-WA-004 Collaboration, D. Aston *et al.*, Nucl. Phys. **B195**, 189 (1982).
- [16] SLAC-BC-072 Collaboration, K. Abe *et al.*, Phys. Rev. D **29**, 1877 (1984).
- [17] HERMES Collaboration, K. Ackerstaff *et al.*, Nucl. Instrum. Methods A **417**, 230 (1998).
- [18] T. Sjöstrand, L. Lönnblad, and S. Mrena, hep-ph/0108264.
- [19] R. Brun, R. Hagelberg, M. Hansroul, and J.C. Lassalle, CERN-DD-78-2-REV, CERN-DD-78-2.
- [20] Particle Data Group, W.M. Yao *et al.*, J. Phys. G:Nucl. Part. Phys. **33**, 1 (2006).
- [21] V. Andreev *et al.*, Nucl. Instrum. Methods A **465**, 482 (2001).
- [22] N. Akopov *et al.*, Nucl. Instrum. Methods A **479**, 511 (2002).
- [23] M. Anselmino, D. Boer, U. D’Alesio, and F. Murgia, Phys. Rev. D **65**, 114014 (2002).
- [24] P.J. Mulders and R.D. Tangerman, Nucl. Phys. **B461**, 197 (1996).
- [25] T.A. DeGrand and H.I. Miettinen, Phys. Rev. D **23**, 1227 (1981); Phys. Rev. D **24**, 2419 (1981); Phys. Rev. D **32**, 2445 (1985).
- [26] K.-I. Kubo and K. Suzuki, in “SPIN 2004: Proceedings of the 16<sup>th</sup> International Spin Physics Symposium and Workshop on Polarized Electron Sources and Polarimeters”, edited by K. Aulenbacher, F. Bradamante, A. Bressan, A. Martin (World Scientific, Singapore, 2005), p. 558.
- [27] M. Burkardt, Phys. Rev. D **66**, 114005 (2002).
- [28] HERMES Collaboration, A. Airapetian *et al.*, Phys. Rev. Lett **94**, 012002 (2005).